Process Safety and Environmental Protection 170 (2023) 1066–1078

Contents lists available at ScienceDirect

Process Safety and Environmental Protection

journal homepage: www.journals.elsevier.com/process-safety-and-environmental-protection

Thermal runaway propagation behavior and energy flow distribution analysis of 280 Ah $LiFePO_4$ battery

Laifeng Song, Zonghou Huang, Wenxin Mei, Zhuangzhuang Jia, Yin Yu, Qingsong Wang, Kaiqiang Jin *

State Key Laboratory of Fire Science, University of Science and Technology of China, Hefei 230026, China

ARTICLE INFO

Keywords:
Lithium-ion battery safety
Thermal runaway propagation
State of charge
Overheating
Heat transfer

ABSTRACT

Thermal runaway propagation (TRP) of lithium iron phosphate batteries (LFP) has become a key technical problem due to its risk of causing large-scale fire accidents. This work systematically investigates the TRP behavior of 280 Ah LFP batteries with different SOCs through experiments. Three different SOCs including 40 %, 80 %, and 100 % are chosen. In addition to key TRP characteristic parameters such as temperature, TRP time and speed are analyzed, more importantly, the energy flow distribution during the TRP of large-size LFP module is also revealed. The results indicate that among the three groups of modules, TRP occurs only in the module with 100 % SOC, which is attributed to the higher internal energy (666.11 kJ) and heat transfer power (264.07 W). For the module with 100 % SOC, the TRP time interval fluctuates from 667 s to 1305 s, and the TRP speed is in the range of 0.05–0.12 mm/s. Furthermore, the energy flow distribution indicates that more than 75 % of the energy is used to heat battery itself, and approximately 20 % is carried out by ejecta. Less than 10 % can trigger neighboring batteries into thermal runaway. This work may provide important guidance for the process safety design of energy storage power stations.

1. Introduction

Energy shortage and environmental pollution have become the main problems of human society, and the protection of the environment and the development of new energy sources have become key research issues worldwide, such as wind, electricity, solar energy, and so on (Wang et al., 2021a). As an energy carrier, lithium-ion batteries (LIBs) have become a promising choice in the field of electrochemical energy storage (EES), considering its high energy density and long cycle life (Bugryniec et al., 2019; Feng et al., 2020). However, in recent years, fire and explosion accidents have occurred frequently in energy storage stations, which have caused catastrophic damage and serious challenges to public safety, such as the Beijing energy storage station accident in April 2021. Usually, fire and explosion accidents are caused by the thermal runaway (TR) of LIBs (Wang et al., 2022b). Meanwhile, numerous accidents have caused substantial property damage and serious social influence.

Numerous experimental pieces of evidence confirm that TR can be easily triggered for the LIB when it is exposed to abnormal operating circumstances, such as mechanical abuse, electric abuse, and thermal abuse (Feng et al., 2018; Wang et al., 2019). In an electrochemical energy storage station, to satisfy the demand for capacity and voltage, a large number of single cells are connected in series and parallel to form a battery module. Typically, the large-format lithium iron phosphate (LFP) battery is commonly used in energy storage stations. In the battery module, once a single cell is triggered to TR, the adjacent cells are easily triggered to TR under huge heat flow and high-temperature ejecta (Wang et al., 2022a; Zhai et al., 2021). According to the domino effect, cell-to-cell thermal runaway propagation (TRP) may occur, which results in serious hazards and threatens people's lives and property. Therefore, TR and TRP have been important problems that need to be explored urgently in the field of LIB safety.

TR is a very complex chemical exothermic reaction, including the decomposition of the SEI film, the reaction of the negative electrode with the electrolyte, and the reaction of the positive electrode with the electrolyte, which generates a large amount of heat, smoke, and gases (Mao et al., 2021; Ping et al., 2015; Wang et al., 2020, 2017). In recent years, scholars have conducted a series of research on the complex

Abbreviations: EES, electrochemical energy storage; LIB, lithium-ion battery; LFP, lithium iron phosphate; TR, thermal runaway; TRP, thermal runaway propagation; SOC, state of charge.

* Corresponding author.
E-mail address: jinkq@ustc.edu.cn (K. Jin).

https://doi.org/10.1016/j.psep.2022.12.082
Received 1 December 2022; Received in revised form 27 December 2022; Accepted 29 December 2022
Available online 31 December 2022

Nomenclature

T	temperature (℃).
V	voltage (V).
t	time (s).
m	mass of battery(g).
A_1	the battery's front surface area (m^2).
A_2	the battery's side surface area (m^2).
E	relative internal energy(kJ).
P	heating power(W).
Q	heat transferred(kJ).
q	heat flow density(W/m^2).
Δt	time interval(s).
v	the TRP speed(mm/s).
R	the thermal resistance of the battery(m^2·K/W).

Greek symbol

c	specific heat capacity(J/kg·K).
ρ	density(m^3/kg).
λ	thermal conductivity(W/m·K).
ε	emissivity.
σ	Boltzmann's constant.
δ	the thickness of the battery(mm).

Subscripts

f	the front surface of the battery.
s	the side surface of the battery.
b	the back surface of the battery.
up	the upper surface of the battery.
i#	the battery label in the module.
cell	the battery in the module.
z	along the cell thickness direction.
sv	safety vent open.
tr	thermal runaway.
max	maximum.
ave	average.
con	convection.
rad	radiation.

chemical exothermic reaction, and explored the behavioral characteristics and influencing factors of TRP based on the TR of a single cell, while proposing various barriers to block TRP. Lamb et al. (Lamb et al., 2015) studied the behavior of thermal runaway propagation of batteries with different battery types and series-parallel connection methods. Lopez et al. (2015) analyzed the effects of cell spacing, circuit connection method and safety valve position on thermal runaway propagation. Feng et al. (Feng et al., 2015a) conducted penetration-induced TR propagation in LIB modules consisting of six LIBs and revealed the TRP mechanism in a large-format lithium-ion battery pack. Based on the analysis, they provided quantified solutions to prevent TRP in the battery pack. Huang et al. (2020) analyzed the TR characteristics of lithium-ion batteries (LIBs) with different states of charge (SOC) and TRP characteristics under different electrical connections by overheating. The research indicated that the TRP is faster in the parallel module than in the series and unconnected modules. Huang et al. (2021b) investigated the characteristics and mechanism of TR and its propagation in LIBs induced by overcharging. The research indicated that TR induced by overcharging exhibits a more severe and catastrophic result. Lai et al. (2021) analyzed and compared the TRP behavior of LIB modules under three typical triggering methods (overheating, nail penetration, and overcharge). They compared the TRP time and TR trigger temperature under the three triggering methods and found that more than 60 % of TR energy is used for battery self-heating and more than 26 % of the energy is emitted. Jia et al. (2022a) studied the characteristics of thermal runaway propagation behavior of two different material batteries under low-pressure environment. The results show that the thermal runaway propagation behavior of cylindrical ternary batteries and lithium iron phosphate batteries in low voltage environments differ greatly. With the environmental pressure decreasing, the thermal runaway propagation of ternary batteries becomes slower, while lithium iron phosphate batteries become faster. For previous relevant work, the researchers have mostly focused on the safety performance of commercial ternary batteries under different abuse conditions (Sun et al., 2022; Wang et al., 2021b). Due to commercial ternary batteries and LFP batteries having significant differences, the conclusions and findings on the TRP of ternary batteries may be not applied to LFP batteries for an energy storage station. To meet the safety performance design in EES, many scientific questions regarding the TR and propagation of $LiFePO_4$ batteries need to be explored and solved, such as the TRP characteristic of format $LiFePO_4$ batteries under different operating conditions.

For TR and its propagation, several scholars have carried out research and exploration. Liu et al. (2021a), (2020) studied the TR characteristics and fire behavior of batteries with different capacities induced by overheating. Mao et al. (2021) carried out experimental research on the TR behavior of a 300 Ah LFP battery and analyzed the fire hazard and gas toxicity of the battery. Zhou et al. (2021) conducted experimental research on the lengthwise/transversal thermal characteristics and jet flow of large-format prismatic $LiFePO_4$ batteries. Huang et al. (2022) systematically investigated the TRP mechanics inside the LFP battery and the influence of the heating position on TR characteristics through experiments. The results indicate that the internal TRP velocity under the bottom and side heating is approximately seven times greater than that under large surface heating. Furthermore, domestic and international scholars have performed much research on cylindrical and prismatic cells with lithium iron phosphate electrodes (Bugryniec et al., 2019; Chen et al., 2019; Duh et al., 2020; Jia et al., 2022a, 2022b; Lei et al., 2017; Liu et al., 2021b; Ouyang et al., 2017; Qin et al., 2022; Wang et al., 2020; Yuan et al., 2020; Zhang et al., 2021). Although some works on the TR of LFP batteries have been performed previously, the most are based on experimental and simulation work related to a single cell. The study of the TRP characteristics and behavior of LFP is still lacking, and the safety issue of EES has still not been fundamentally solved. The TRP characteristic of large-format $LiFePO_4$ batteries is still an extremely critical issue. Zhou et al. (2022) designed battery modules with different connection modes using 50 Ah $LiFePO_4$ batteries to reveal TRP mechanisms. Compared with the module without connection, the parallel module released much higher heat flux to adjacent batteries, leading to shorter TR propagation time and more severe TRP. However, there is no clear conclusion on the TRP characteristics of larger-capacity $LiFePO_4$ batteries with different SOCs. At the same time, there is no in-depth study about the energy flow distribution when the TR occurs for LFP battery. Thermal runaway propagation characteristics have certain guiding role and reference significance for the process safety management of energy storage batteries. Research on the TRP behavior of large-format $LiFePO_4$ batteries will be very meaningful and instructive for the safety performance design and operation in energy storage stations.

This paper aims to fill the knowledge gap about the TRP characteristics of large-format $LiFePO_4$ batteries with different SOCs and reveal the energy flow distribution during the TRP. Numerous external heating experiments were performed based on 280 Ah prismatic batteries under different SOCs to investigate the TRP phenomenon in the battery module. Some typical TR characteristic parameters, such as temperature, voltage, and mass loss under different experimental conditions were

Table 1
The essential parameters of the tested LFP battery.

Name	Unit	Value
Cathode	-	Lithium phosphate ($LiFePO_4$)
Anode	-	Graphite
Dimension(length×height×thickness)	mm^3	175 × 205 × 72
Nominal capacity	Ah	≥ 280
Mass	g	5435 ± 100
Nominal voltage	V	3.2
Charge and discharge voltage	V	2.5–3.65
State of charge	%	40, 80, 100
Specific heat capacity	J/(kg·K)	1029.49
Density	kg/m^3	2118
Thermal conductivity	W/(m·K)	X/Y/Z:21.63/21.63/2.11

analyzed in detail. In addition, the TR propagation features of the large-format LFP battery were comparatively analyzed. Finally, the energy flow distribution during the TRP was quantified from the calculated energy value.

2. Experimental

2.1. The battery sample

In this study, a kind of 280 Ah commercial prismatic battery was used. The cathode active material is $LiFePO_4$ composite cathode, and the anode is graphite. The cell is 175 × 205 × 72 mm in size, and its weight is 5435 ± 100 g. The capacity of the cell is about 280 Ah with a nominal voltage of 3.2 V, and the cut-off voltages are 3.65 V and 2.5 V for charging and discharging respectively. Some other physical parameters of the LIB are listed in Table 1. All tested batteries were charged fully using a battery cycler (NEWARE CT-4008–5V20A-A) before the experiment.

C-rate is the measurement of the charge and discharge current with respect to its nominal capacity. It refers to the current value required to charge the battery to its rated capacity within a specified time, which is numerically equal to the multiple of the battery's rated capacity (Huang et al., 2022). Each tested battery was discharged to 2.5 V with a constant current of about 0.07 C (20 A) and then charged to 40 % SOC, 80 % SOC, or 100 % SOC at a rate of 20 A with a constant current and constant voltage. After charging and discharging were completed, the plastic packaging on the surface of the LIBs was removed from all cells before testing. The initial mass of the LIBs without packaging was recorded.

2.2. Thermal runaway propagation tests of three cells

Fig. 1(a) showed the experimental platform used in the work, including a combustion chamber fabricated following ISO9705 with the dimensions of 1.8 m × 1.8 m × 2 m and some other experimental equipment. There was a smoke exhaust duct on the upper side of the combustion chamber. To monitor the content and concentration of the smoke and gas in real-time, a Fourier Transform Infrared Spectrometer (FTIR Spectrometer) was employed. All experiments were performed in the combustion chamber.

The experimental sample was three cells in close contact with the

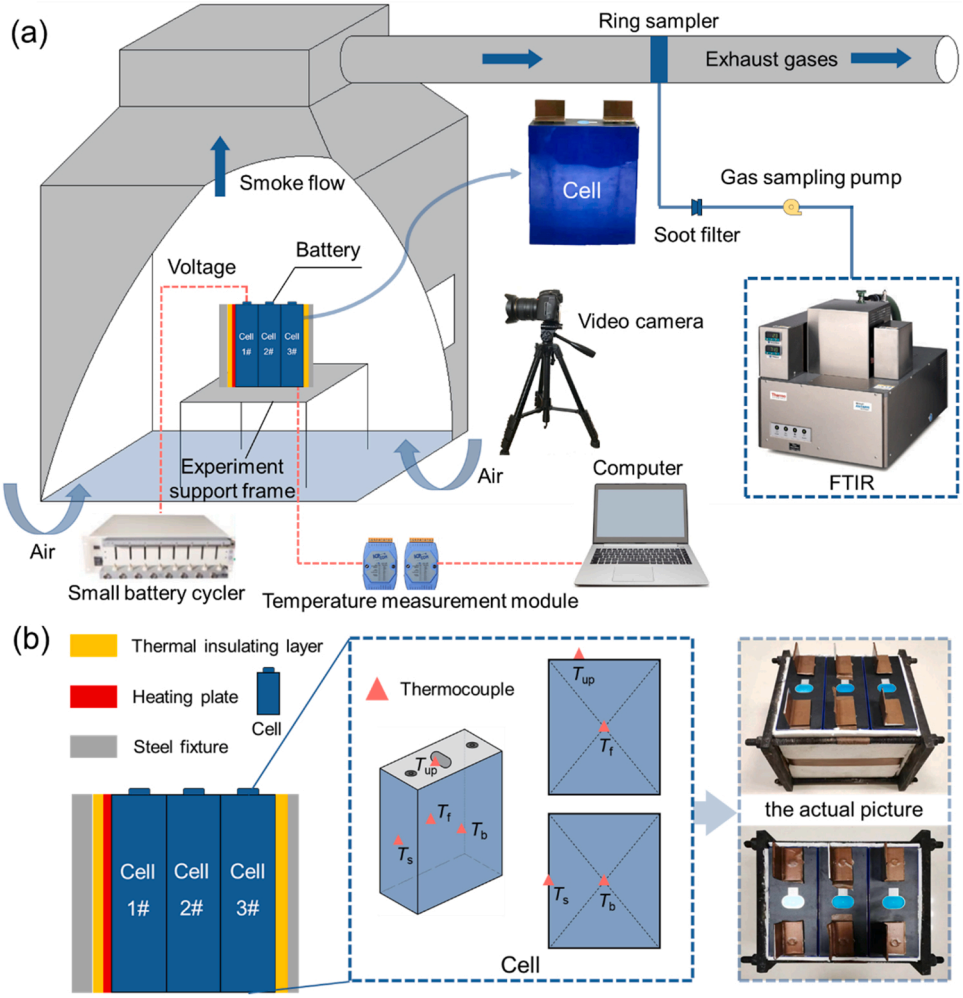

Fig. 1. (a) Experimental setup for the thermal runaway propagation tests with different SOCs. (b) Schematic of three cells and the arrangement of the thermocouples.

Table 2
Experimental specifications and test schedule.

Experiment No.	SOC	The number of cells	Heater power/W
1	40 %	3	500
2	80 %	3	500
3	100 %	3	500
4	100 %	5	500

same SOC. Cell i# ($i = 1, 2, 3$) was used to describe the three cells. All cells were placed in an experimental support frame and fixed by a steel fixture to ensure consistent conditions for each experiment. As shown in Fig. 1(b), the red represented a 500 W heating plate with the same sidewall size as the tested cell. The yellow was the thermal insulating layer that was used to heat dissipation between the battery and the heating plate to the steel fixture. Three K-type thermocouples with a diameter of 1 mm were attached to the surface of each battery using high temperature resistant tape, including the front surface as T_f, the side surface as T_s, and the back surface as T_b, to measure the surface temperature. One thermocouple was placed near the safety vent named T_{up}. Owing to the limited measurement accuracy, the temperature acquired by the thermocouples had an error of ± 2.5 ℃. All temperature data were recorded by the data acquisition equipment (ICPCON I-7018), and the voltage of the cell 1# was recorded by a Neware battery cycler. In addition, during the test, a video camera (SONY XPS160) at 50 Hz was used to monitor TR and propagation behavior and the gas injection phenomenon. Mettler balance was used to measure the mass of the battery before and after each experiment.

Three experiments triggered by a 500 W heating plate were carried out to explore the SOC effect on TRP. In order to reduce the influence of the attenuation of heating power, the heating plate was updated after each experiment. In the scenario of LIB transportation, the battery is usually at 40 % SOC. During the operation of the energy storage station, the battery is usually at approximately 80 % SOC. Moreover, the battery at 100 % SOC is one of the most dangerous conditions under normal operation. Therefore, 40 % SOC, 80 % SOC, and 100 % SOC were selected for comparison, corresponding to experiments No.1, No.2, and No.3 in Table 2. Some critical parameters of cells with different SOCs, including surface temperature, the voltage of cell 1#, and the mass were obtained to explore the TR and propagation behavior of the battery with different SOCs.

2.3. Thermal runaway propagation tests of the battery module

Considering the hazard and risk of the TR of the LIBs, the propagation behavior and characteristics can not be reflected through the TRP test of three cells when the TR occurred in a real module. The TRP tests on a small LIB module with five cells were conducted in the combustion chamber. A schematic of the tested small module that formed with five cells (cell 1# ~ cell 5#) was shown in Fig. 2. Five cells were held in a steel fixture. Cell i# ($i = 1, 2, 3, 4, 5$) was used to define these five LIBs with 100 % SOC. All the tested cells were wrapped with the thermal insulating layer, and cell 1# was heated by a 500 W heating plate until TR. The test process was recorded using a video camera (SONY XPS160) at 50 Hz through a viewing window.

For each cell in the small module, four thermocouples were attached to the surface of each cell to obtain its temperature variation. T_{if} ($i = 1, 2, 3, 4, 5$) was used to describe the temperature of the battery front surface. It should be noted that $T_{1\,f}$ referred to the temperature between the heating plate and cell 1#. Since $T_{1\,f}$ was the temperature close to the heating plate, $T_{1\,f}$ marked the temperature of the front surface of cell 1#, which can also represent the surface temperature of heating plate before TR. The back surface temperature of the cell was represented by T_{ib} ($i = 1, 2, 3, 4, 5$). Meanwhile, the temperature of the side surface and

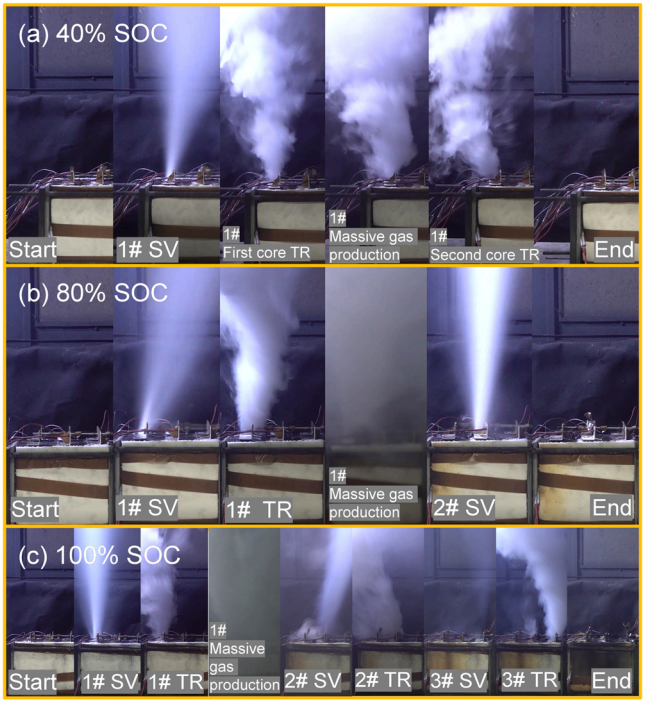

Fig. 3. The TR and its propagation phenomenon of LFP batteries with different SOCs: (a) 40 % SOC; (b) 80 % SOC; (c) 100 % SOC.

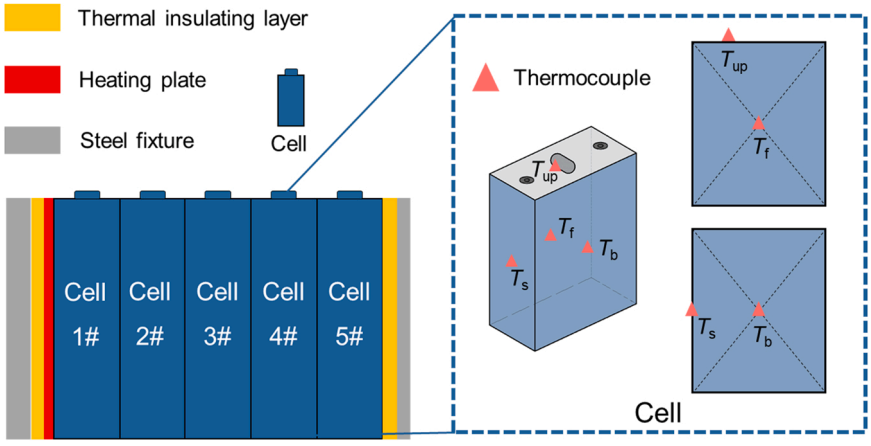

Fig. 2. Schematic of the battery module and the thermocouple arrangement in the TRP tests with five cells.

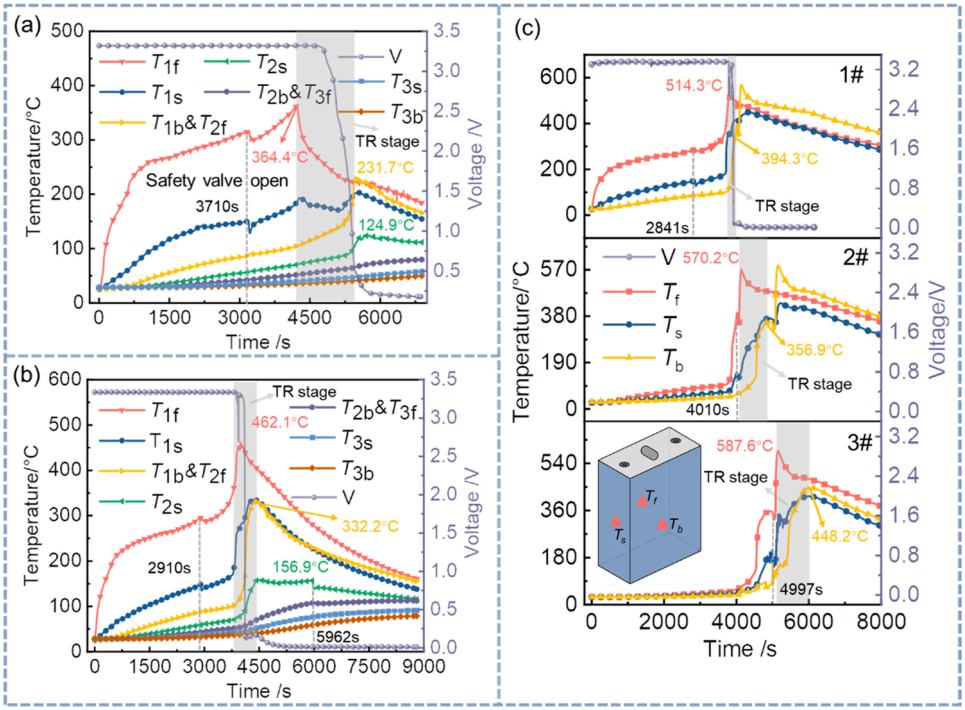

Fig. 4. Temperature and voltage curves for cells with different SOCs: (a) 40 % SOC; (b) 80 % SOC; (c) 100 % SOC.

near the safety vent of the cell were defined by T_{is} and T_{iup} (i = 1, 2, 3, 4, 5).

3. Results and discussion

3.1. TRP tests of the three cells with different SOCs

3.1.1. Thermal runaway behavior of batteries with different SOCs

The TR and propagation behavior of the 280 Ah LFP battery is shown in Fig. 3 under 40 % SOC, 80 % SOC, and 100 % SOC. According to the experimental phenomena, different TRP characteristics are observed for batteries with different SOCs. The 40 % and 80 % SOC batteries do not show TRP phenomena, and TR only occurs in cell 1#, while all three cells with 100 % SOC experience TR.

As shown in Fig. 3, the test is over when cell 1# is completely out of thermal runaway for the battery with 40 % SOC. The time interval is longer between the TR occurrence of the first and second rolled core, and the exhaust duct can quickly carry away the generated smoke and gases during the TR. Compared with the 80 % and 100 % SOC cases, the lower SOC results in a slower gas production rate and less gas production volume for the battery with 40 % SOC. For the battery with 80 % SOC, the TRP phenomena are similar to the case of 40 % SOC, and the differences are mainly manifested in two aspects. On the one hand, the gas production behavior is more severe in the TR stage. On the other hand, after cell 1# completely TR for a while, the safety vent of cell 2# is opened due to the higher electrolyte vapor pressure inside cell 2# (Jia et al., 2022b). For the battery with 100 % SOC, cell 1#, cell 2#, and cell 3# undergo thermal runaway in turn generating a large amount of smoke and gases.

Table 3
Mass loss of cells before and after testing with different SOCs.

Experiment No.	Cell *i*#	Mass before test/g	Mass after test/g	Mass loss/g	Mass loss rate/%
1	1#	5448.8	4529.4	919.4	16.87 %
2	1#	5450.3	4365.3	1085	19.91 %
	2#	5460.1	4900	560.1	10.26 %
3	1#	5460.3	4267.9	1192.4	21.84 %
	2#	5456.3	4307.5	1148.8	21.05 %
	3#	5469.1	4320.8	1148.3	21.00 %

3.1.2. Analysis of thermal runaway parameters

In TR evaluation and early warning about large-format batteries, the surface temperature and voltage are the essential data (Jin et al., 2020; Li et al., 2019). The process of safety vent opening can eject a large amount of electrolyte (Feng et al., 2018; Zhao et al., 2021). When an internal short circuit occurs in the battery, the chemicals inside the cell may undergo a variety of chemical reactions to produce gases (Mathieu et al., 2022). These processes result in mass loss. Therefore, mass loss is also an important parameter for the risk assessment of TR.

Fig. 4 illustrates the cell's surface temperature and voltage of cell 1# in the process of TRP. As shown in Fig. 4, when the SOC is 40 % for the LFP battery, the maximum temperature is 364.4 ℃ on the front surface and 231.7 ℃ on the back surface. It is worth noting that the voltage drops slowly until it reaches 0 V after TR is over. Meanwhile, the side surface temperature of cell 2# increases to 124.9 ℃ and finally decreases slowly. For the 80 % SOC, a steep temperature rise occurs on the front, side, and back surfaces of the cell sequentially. The voltage of cell 1# drops rapidly to 0 V when the back surface temperature rapidly rises. The maximum temperatures are 462.1 ℃ and 332.2 ℃ on the front and back surfaces, respectively. Compared to experiment No.1, the safety vent of cell 2# is opened at 5962 s in experiment No.2, in which the side temperature of cell 2# is 156.9 ℃. However, cell 2# does not undergo TR, which means no TRP occurs.

Experiment No.3 is significantly different from experiments No.1 and No.2. There is a steep temperature rise in all three cells, and the maximum temperature is higher than that in the 40 % and 80 % SOC cells, as shown in Fig. 4. For the LFP battery with 100 % SOC, the maximum temperature of the front surface exceeds 500 ℃ in the TRP experiment. Due to the close contact between cells, a large amount of heat is transferred from cell *i*# to cell $i+1$# when thermal runaway occurs. The temperature on the back of cell 1# and cell 2# is lower, corresponding to 394.3 ℃ and 356.9 ℃ respectively. However, the maximum temperature on the back surface of cell 3# is 448.2 ℃

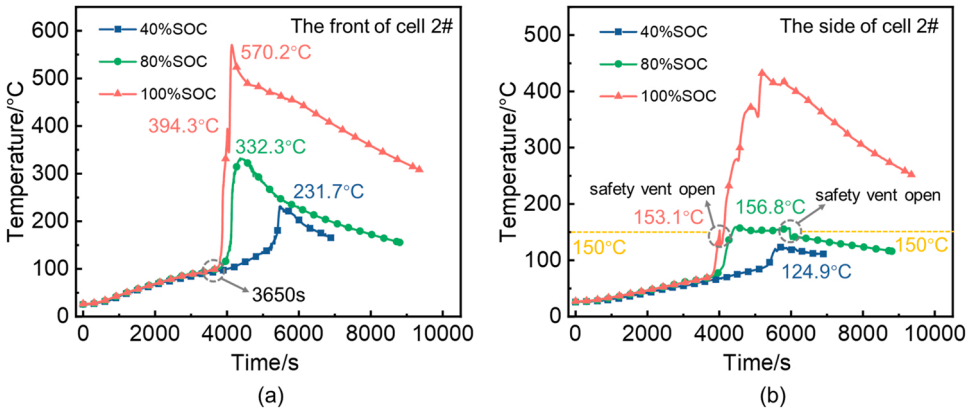

Fig. 5. The surface temperature curve for cell 2# in TR propagation: (a) the front of cell 2#; (b) the side of cell 2#.

because the back surface of cell 3# is wrapped with the thermal insulation layer.

All tested batteries are weighed before and after the experiment, and the mass loss and the mass loss rate are calculated, as shown in Table 3. The mass loss rate is 16.87 % for the battery with 40 % SOC; nevertheless, the battery with 80 % and 100 % SOC are 19.91 % and 21.84 % respectively. It can be found that the SOC is higher, the reaction inside the cell is more complete and the mass loss is greater. In experiment No.2, the safety vent is opened for cell 2# and does not experience TR, so the mass loss rate is only 10.26%, which is approximately 50% of the mass loss rate of cell 1#. Therefore, the safety vent opened can remove more material, occupying approximately half of the total mass loss.

Comparing the safety vent opening time, the maximum temperature, and the mass loss during TR for cell 1# in each group of experiments, we can obtain the following conclusions: (a) With the increase of SOC, the safety vent opening time gradually become shorter, and the maximum temperature of the cell surface gradually increases when TR occurs. (b) With the increase of SOC, the mass loss of the battery linearly increases, and the mass loss rate is approximately 21.5 % after TR. (c) The higher the state of charge is, the more likely the TRP occurs. In a specific external environment, there is a critical TRP state of charge in theory.

3.1.3. *Analysis of the reasons for nonspread*

When TR occurs in cell 1#, the cells with 40 % and 80 % SOC do not continue to trigger TR in cell 2#. However, the cell with 100 % SOC shows a continuous propagation phenomenon. The section will explain this phenomenon in terms of battery surface temperature and heat transfer. Fig. 5 illustrates the surface temperature curve for cell 2# during TR propagation. The cell with 100 % SOC has a higher temperature in Fig. 5. According to the theory of heat conduction, heat is always transferred from high-temperature to low-temperature objects under the condition of no external interference, and the greater the temperature difference, the more heat is transferred at the same time. Therefore, cell 2# with 100 % SOC can receive more heat, which makes it can be triggered into TR.

Temperature can characterize the heat of the battery. Based on extensive experimental data, the temperature on the side of the battery is around 150 ℃ or even higher when the safety vent is open, and it is defined as T_{sv}. For cell 2# in experiments No.2 and No.3, T_{sv} is 153.1 ℃ and 156.8 ℃ respectively, while the maximum temperature on the side of cell 2# with 40 % SOC is only 124.9 ℃. The temperature does not reach the threshold of the safety vent opening. When the safety vent opened, a large amount of heat is removed, which results in the battery temperature reduction. Meanwhile, the remaining heat inside the battery is not enough to trigger the TR, so the surface temperature of the battery continues to decrease.

Because the thermal conductivity along the thickness direction of the battery λ_z is only 2.11 W/(m·K), there is a large temperature gradient

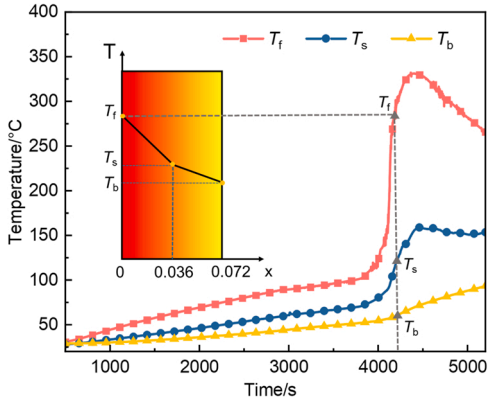

Fig. 6. Temperature distribution of cell 2# at the moment before TR occurs.

along the thickness direction of cell 2# before TR occurs. The temperature of the battery surface is obtained experimentally as T_f, T_s, and T_b. Since the analytical solution of the temperature field of the nonstationary thermal conductivity process is complex, it is assumed that the temperature inside the battery varies linearly along the thickness direction. There are two rolled cores inside the battery, and there is contact thermal resistance between the two rolled cores. Therefore, the temperature variation along the thickness direction is represented in Fig. 6, and the temperature at a moment along the cell thickness direction before TR occurs can be calculated by Eq. (1):

$$T\left(\begin{array}{c} x,t \end{array}\right) = \begin{cases} \dfrac{T_s - T_f}{0.036}x + T_f & 0 \le x \le 0.036 \\ \dfrac{T_b - T_s}{0.036}(x - 0.036) + T_s & 0.036 \le x \le 0.072 \end{cases} \tag{1}$$

where T_f is the battery's front surface temperature, and T_s and T_b are the battery's side and back surface temperature, x represents the distance along the battery thickness direction.

The internal energy change in the battery (E_{cell}) at a moment before TR occurs can be determined by Eq. (2):

$$E_{cell}(t) = \int_0^{0.072} c_b A_1 \rho_b \left(T(x,t) - T_{0,cell}\right) dx \tag{2}$$

where c_b and ρ_b are the specific heat capacity and density of the battery, A_1 is the battery's front surface area, $T(x,t)$ is the temperature distribution of the battery along the thickness direction, and $T_{0,cell}$ is the average temperature of the battery surface at the initial moment, as shown in Eq. (3). The initial moment will be explained next.

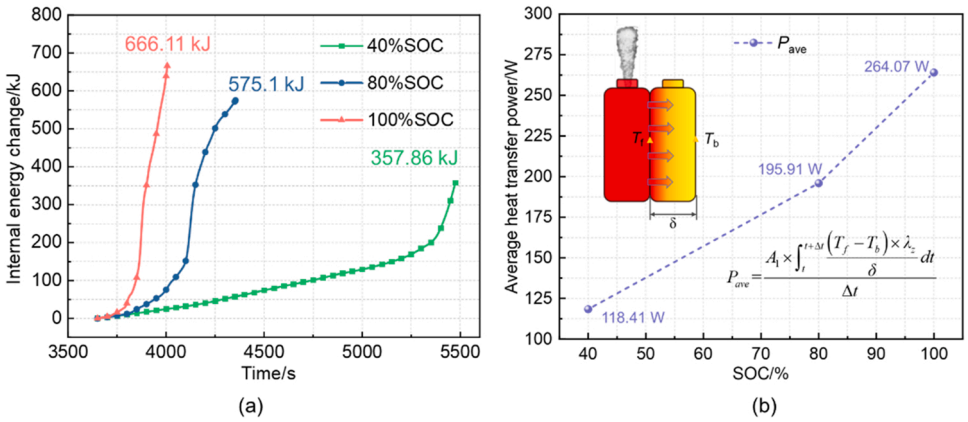

Fig. 7. The key parameters for the cell with different SOCs during the TRP: (a) Internal energy change of cell 2# with different SOCs; (b) Heat transfer power from cell 1# to 2#.

$$T_{0,cell} = \frac{T_f + 2T_s + T_b}{4} \tag{3}$$

According to Fig. 5, the front surface temperature of cell 2# is almost the same for different SOCs before 3650 s, while different trends in the front surface temperature of cell 2# are presented for the three operating conditions after 3650 s. Therefore, a period of time from 3650 s to the moment that cell 1# is completely out of the TR is chosen to calculate the relative internal energy in cell 2# and $T_{0,cell}$ represents the temperature at the moment of 3650 s, as shown in Fig. 7(a). At the end of the TR with cell 1#, the relative internal energy of cell 2# with 100 % SOC is 666.11 kJ, which is much higher than that of 40 % and 80 % SOC cases. Except for the relative internal energy, according to Fourier's law of thermal conductivity, the average heat transfer power between cell 1# and cell 2# is also calculated by Eq. (4), where Δt stands for a while after the rapid temperature rise of the back surface of cell 1#, A_1 represents the area of the large surface of the cell, T_f and T_b the temperatures of the front and back surfaces of the cell, respectively. λ_z and δ are the thermal conductivity along the cell thickness direction and the thickness of the battery.

$$P_{ave} = \frac{A_1 \times \int_t^{t+\Delta t} \frac{(T_f - T_b)\times\lambda_z}{\delta} dt}{\Delta t} \tag{4}$$

The average heating power gradually decreases as the SOC decreases, and less energy is stored inside cell 2# per unit of time. This is because the TR reaction with a higher SOC is more severe and can generate more heat, causing more heat to be transferred to the next battery, as shown by the higher heat transfer power of cell 2#. The average heating power is 118.41 W, 195.91 W, and 264.07 W for 40 %, 80 % and 100 % SOC, respectively. Through the above analysis, it can be found that for the battery with 40 % and 80 % SOC, the generated energy during the TR is not enough to trigger TR in the next battery compared to the case of 100 % SOC, and the average heat transfer power is relatively low. Therefore, when the SOC is low, the TRP phenomenon may not occur in a battery module.

3.2. TRP features of the battery module with five cells

According to the analysis in Section 3.1, it can be found that the SOC has an influence on the TRP, and complete TRP occurs under 100 % SOC conditions. However, it is difficult to obtain the TRP characteristic by experiment No.3. Thus, the TRP characteristic of the battery module with five cells will be analyzed in this section.

3.2.1. Temperature response of cells during thermal runaway propagation

According to the experimental phenomenon and the temperature change curve of the cell surface, it can be concluded that TR occurs in all five cells. After TR occurs in cell 1#, the TR behavior gradually spreads to cell i# (i = 1, 2, 3, 4) along the battery arrangement direction. The TRP process can be divided into five stages. The temperature response of the cells in the module during TR propagation is shown in Fig. 8. The steep temperature rise occurs on the front, side, and back surfaces from cell 1# to 5# sequentially. The gray area indicates the TR stage for each cell from the moment the safety vent is opened to the maximum temperature of the TR.

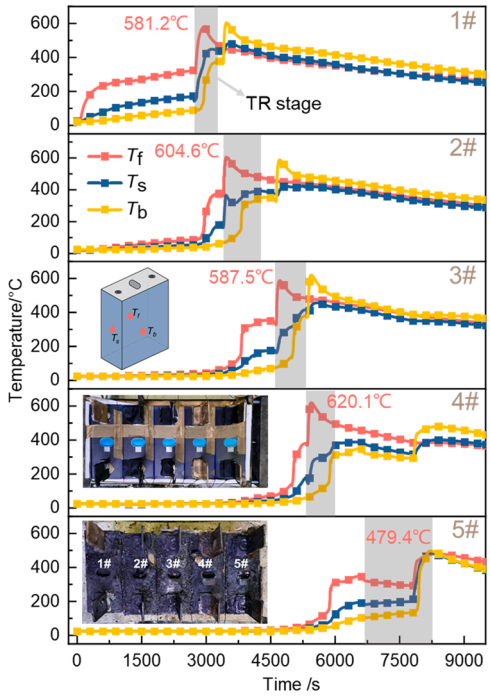

Fig. 8. Temperature response of the five cells during TR propagation.

Stage I: Cell 1# is overheated continuously and the front surface temperature increases steadily. The safety vent is opened at 2237 s due to a large pressure difference inside and outside the battery. The pressure difference is mainly attributed to the electrolyte vapor inside the battery. During the opening of the safety vent, a large amount of electrolyte is ejected to take away part of the heat inside cell 1#, and the surface temperature decreases. As the temperature continues to rise, TR occurs at 2751 s for cell 1#, with a sharp temperature rise on the front and back surface in sequence. The maximum surface temperatures are 581.2 ℃ and 376.1 ℃ on the front and back surfaces, respectively.

Table 4
The characteristic parameters of the TRP process.

Cell *i*#	t_{sv}/s	t_{tr}/s	T_{tr}/℃	T_{f_max}/℃	T_{b_max}/℃
1#	2704	2750	146.1	581.2	376.1
2#	3371	3396	162.3	604.6	354.7
3#	4603	4630	164.1	587.5	380.9
4#	5332	5358	143.6	620.1	348.2
5#	6637	7805	201.5	479.4	497.6

Stage II: After TR occurs in cell 1#, the side surface temperature of cell 2# reaches 180.6 ℃ due to heat transfer. Immediately, the safety vent is opened and the TR occurs. It can be found that the temperature of the front and back surfaces in cell 2# does not increase rapidly at the same time, while the time interval is approximately 400 s. This fully indicates that there are two rolled cores inside the battery, and TR occurs sequentially in the two rolls, rather than simultaneously. In addition, it is found that the TRP phenomenon also occurs inside the battery. View from the temperature curve of cell 1#, it can be found that the side temperature of cell 1# gradually increases when TR occurs in cell 2#. At the same time, the surface temperature of cell 3# also increases, which indicates that when TR occurs in one battery, the heat generated by the battery can be transfer to the next and previous battery by heat conduction.

Stages III and IV have the same process as Stage II. The two roll cores occur TR sequentially after the opening of the safety vent. The characteristic parameters of the TR process are shown in Table 4.

Stage V: Due to the quality problem of the safety vent, the time interval is 1187 s between the safety vent opened and the TR triggered for cell 5#. At 6689 s, a tiny crack appears at the safety vent of cell 5#, and a large number of gases generated inside the battery is released through

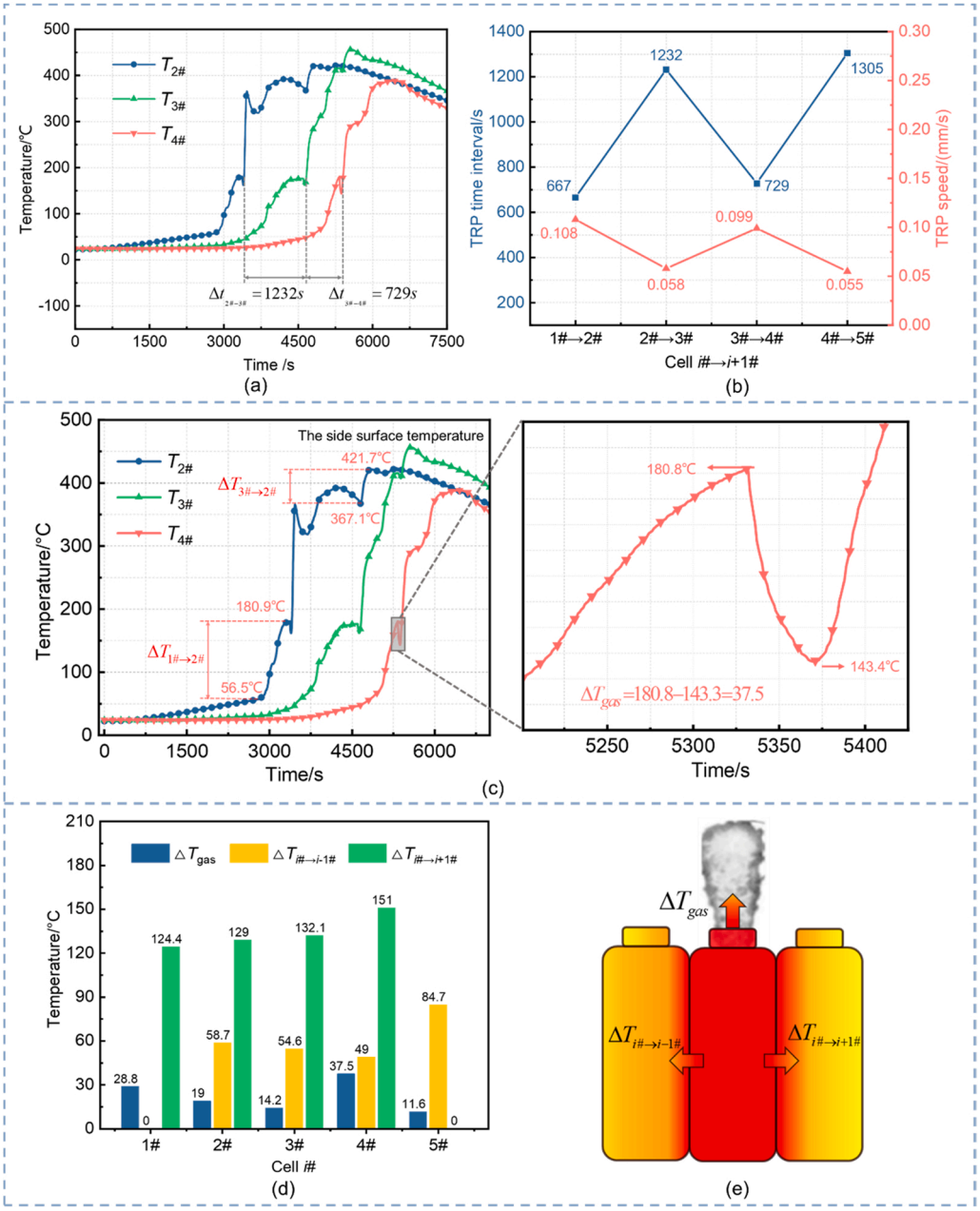

Fig. 9. The calculation process and results of TRP characteristic analysis: (a) Schematic of TRP time interval; (b) TRP time interval and speed for the module with five cells; (c) Schematic diagram of qualitative analysis of energy flow; (d) The side surface temperature variation of each battery in the TR stage; (e) Schematic of the heat transfer path between adjacent cells in terms of the temperature change.

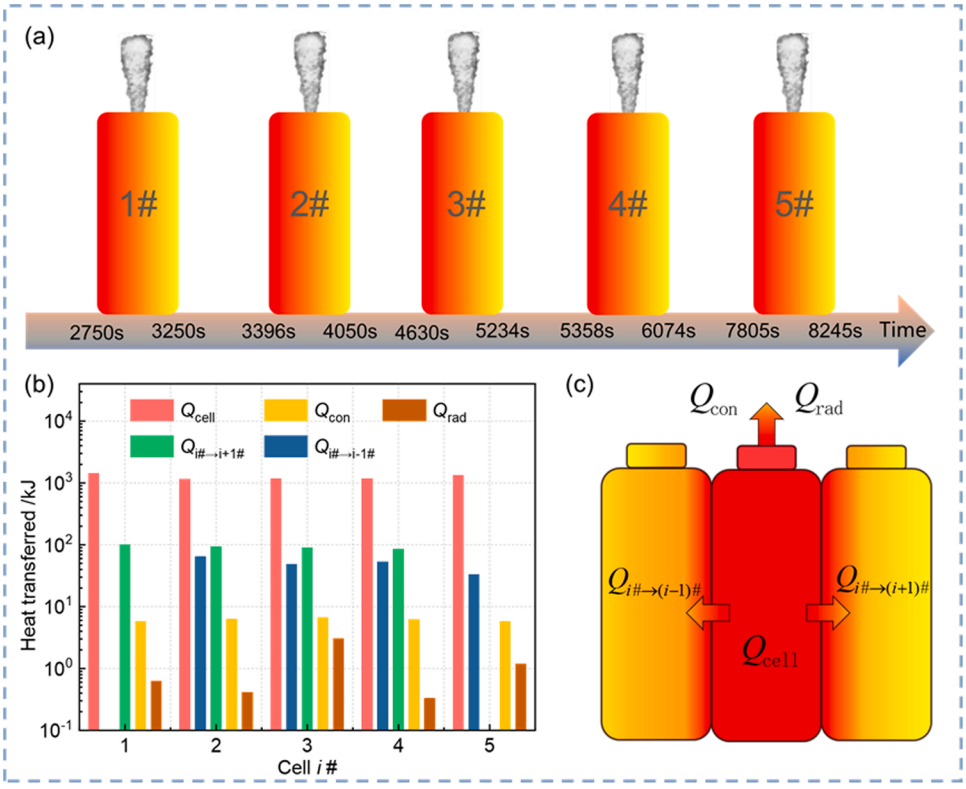

Fig. 10. Schematic diagram of energy flow analysis and results: (a) Time-sequence diagram of the TR for the module with five cells during the TRP. (b) The energy value of the transferred heat through three heat transfer paths during the TRP. (c) Schematic of the heat transfer path between adjacent cells in terms of the energy distribution.

the crack. Then the internal reaction of cell 5# gradually accelerates, the internal pressure exceeds the maximum value, the safety vent is broken at 7169 s, and TR immediately occurs ejecting a large amount of gas and smoke. The maximum temperature on the back surface of cell 5# is higher than that of the other cells due to the back surface of cell 5# being the insulation layer, so the generated heat inside the battery can not be transferred downstream, producing a heat accumulation effect.

3.2.2. Analysis of thermal runaway propagation characteristics

In general, the parameters used to describe the TRP characteristics are the TRP time interval, the TRP speed, the energy flow direction of the TRP, and so on. According to the analysis in Section 3.2.1, we find that TR occurs immediately after the safety vent is opened (except for cell 5#), so the TRP time interval is defined as the time difference when the temperature rapid rise in the side-surface center point of two adjacent cells by Eq. (5), usually at a temperature rise rate greater than 1 ℃/s, where $t_{s\_i\#}$ represents the time when the temperature rise rate of the side-surface center point is greater than 1 ℃/s for cell i#. Meanwhile, the TRP speed is defined by Eq. (6), in which δ_{cell} is the distance between the two cell-side surface center points. Fig. 9 illustrates the experimental results of the TRP time interval for the module with five cells. It can be found that the TRP time interval fluctuates, and it is not a gradually increasing or decreasing situation. This phenomenon also appears in Ref. (Huang et al., 2021a; Zhou et al., 2022) and may be related to battery expansion during TR propagation. The relationship between the spacing between cells and the contact thermal resistance is described in Ref. (Jia et al., 2020). For a period of time before the battery was triggered to TR, a large amount of electrolyte vapor is generated inside the battery causing the battery to expand and crush the adjacent battery. The dynamic change in contact thermal resistance between cells affects the heat transfer between cells. Therefore, the dynamically changing contact thermal resistance leads to uncertainty in the heat transfer between cells and further fluctuating changes in the TRP time. In addition, the TRP speed is calculated according to Eq. (6). The TRP speed is in the range of 0.05–0.12 mm/s, which is less than the calculated internal TR propagation speed in Ref. (Huang et al., 2021a).

$$\Delta t_{i\#\to i+1\#} = t_{s\_i+1\#} - t_{s\_i\#}, i \in \{1,2,3,4\} \tag{5}$$

$$v_{i\#\to i+1\#} = \frac{\delta_{cell}}{\Delta t_{i\#\to i+1\#}} \tag{6}$$

As the battery is composed of various materials, the thermophysical parameters are anisotropic and the battery interior has a large temperature difference, it is more difficult to accurately calculate the heat received by the battery, so the temperature change of the battery surface is used to qualitatively measure the heat transfer relationship between the cells. It is assumed that the front surface of cell 1# and the back surface of cell 5# are adiabatic, and the surface temperature change is used to characterize the energy distribution of the battery's heat production. The heat dissipation from the battery to the surrounding environment or the battery is composed of three parts, and the calculation process can be found in Fig. 9. Based on the previous assumption, the change of the cell surface temperature due to heat transfer during the TRP is calculated. Fig. 9 shows the relative magnitude of heat transfer in the three heat dissipation paths. It can be found that less heat is carried away by the electrolyte spray, and the heat transferred from cell i# to (i + 1) # is an order of magnitude greater than the heat transferred to (i-1) # in terms of the value of the temperature change. This is because there is a large temperature gradient between the cells. When TR occurs in cell i#, cell i# transfers more heat to cell (i + 1) #, which is at a lower temperature than cell (i-1) #. However, the heat taken away by the TR gas production process is not expressed qualitatively, and the radiation and convection heat transfer is not represented.

3.2.3. Heat transfer and distribution between adjacent batteries

For a lithium battery module, numerous studies have indicated that

heat transfer through radiation and convection accounts for a small proportion of the total heat transfer (Feng et al., 2015b; Li et al., 2019). Therefore, the heat transfers from cell $i\#$ to cell $i+1\#$ mainly through the thermal conductivity on the contact surface of the aluminum shell. It is assumed that the LFP is a uniform mass of solid, the internal flow of the medium and heat transfer inside the battery are not considered. The TR battery is regarded as a uniform heat source, and the solid heat transfer is the main calculation of heat flow in the TRP process. Because no jet flame is produced in the experimental process, the effect of the flame on the TRP of heat transfer can be ignored here.

The energy flow is divided into five parts during the TRP, including the Q_{cell} used to heat the cell itself, the $Q_{i\#\rightarrow(i+1)\#}$ transferred to the next cell, the $Q_{i\#\rightarrow(i-1)\#}$ transferred to the previous cell, the heat dissipated to the surrounding environment by convection and radiation, and the heat taken away by the TR gas production process. A schematic of the heat transfer path between adjacent cells is presented in Fig. 10. Since TR gas production is a dynamic change process, the heat taken away by the TR gas production is not quantitatively calculated in this section. Accurate calculation of the heat carried away by the gas generated during thermal runaway is a key research element in the future.

According to Fourier's law of thermal conductivity (Li and Ostanek, 2023; Yan et al., 2021), the heat flux inside the battery can be obtained through Eq. (7), where R_{cell} is the thermal resistance of the battery, which can be calculated by Eq. (8), and the parameters can be obtained in Table 1. Furthermore, the heat transfer through the contact surface can be roughly calculated by Eq. (9) and Eq. (10) from cell $i\#$ to cell $(i+1)\#$ or $(i\text{-}1)\#$ when the TR occurs in cell $i\#$, where the value of A_1 is 0.035875 m^2.

$$q_{i\#}(t) = \frac{|T_{if} - T_{ib}|}{R_{cell}}, i = \{1,2,3,4,5\} \tag{7}$$

$$R_{cell} = \frac{\delta}{\lambda_z} \tag{8}$$

$$Q_{i\#\rightarrow(i-1)\#} = A_1 \times \int_{t_0}^{t_1} q_{i-1}(t)dt \tag{9}$$

$$Q_{i\#\rightarrow(i+1)\#} = A_1 \times \int_{t_0}^{t_1} q_{i+1}(t)dt \tag{10}$$

According to Newton's law of cooling and Boltzmann's law, the heat flux can be obtained through Eq. (11) and Eq. (12). The heat flow density is integrated at a specific time to obtain the convective and radiative heat exchange during the thermal runaway phase, as shown in Eq. (13) and Eq. (14), where the value of A_2 is 0.0126 m^2. In addition, the heat caused by the temperature rise of the battery is calculated through Eq. (15).

$$q_{con}(t) = h \times \left(T_{up} - T_{\infty}\right) \tag{11}$$

$$q_{rad}(t) = \varepsilon_{rad} \times \sigma_{rad} \times \left(T_{up}^4 - T_{\infty}^4\right) \tag{12}$$

$$Q_{con} = A_2 \times \int_{t_0}^{t_1} q_{con}(t)dt \tag{13}$$

$$Q_{rad} = A_2 \times \int_{t_0}^{t_1} q_{rad}(t)dt \tag{14}$$

$$Q_{cell} = c \times m \times \Delta T \tag{15}$$

The thermal runaway time node of the battery is divided to obtain the time sequence diagram according to the temperature variation curve in Section 3.2.1. When the temperature rise rate of the front surface measurement point of the battery reaches 1 ℃/s, it is the moment when the TR of the battery starts. When the temperature measurement point on the back surface of the battery reaches the maximum value or the temperature rate starts to decrease below 1 ℃/s, we consider the moment as the end of TR. The time sequence diagram is shown in Fig. 10. During the TR of each battery, the value of the transferred heat through three heat transfer paths is illustrated in Table 5. As the front surface of cell 1# is close to the heating plate and the back of cell 5# is wrapped with the thermal insulating layer, the Q_{cell} used to heat the cell itself is higher than the other three cells. Due to the large temperature gradient between adjacent cells, the heat transfer to the next cell is greater than the previous cell. Fig. 10 presents the relationship between the magnitude of the energy values. For all the calculated heat, the heat through convection and radiation is lower compared to other heat. From the view of orders of magnitude, the energy of radiation and convection

Table 5
The calculated value of the energy through three heat transfer paths during the TR of each battery.

Cell $i\#$	Q_{cell}/kJ	$Q_{i\#\rightarrow(i+1)\#}$/kJ	$Q_{i\#\rightarrow(i-1)\#}$/kJ	Q_{con}/kJ	Q_{rad}/kJ
1#	1432.67	100.33	—	5.782	0.628
2#	1152.21	93.45	64.58	6.277	0.414
3#	1163.40	89.41	48.79	6.632	3.042
4#	1173.89	85.40	53.45	6.242	0.329
5#	1319.23	—	33.01	5.818	1.195

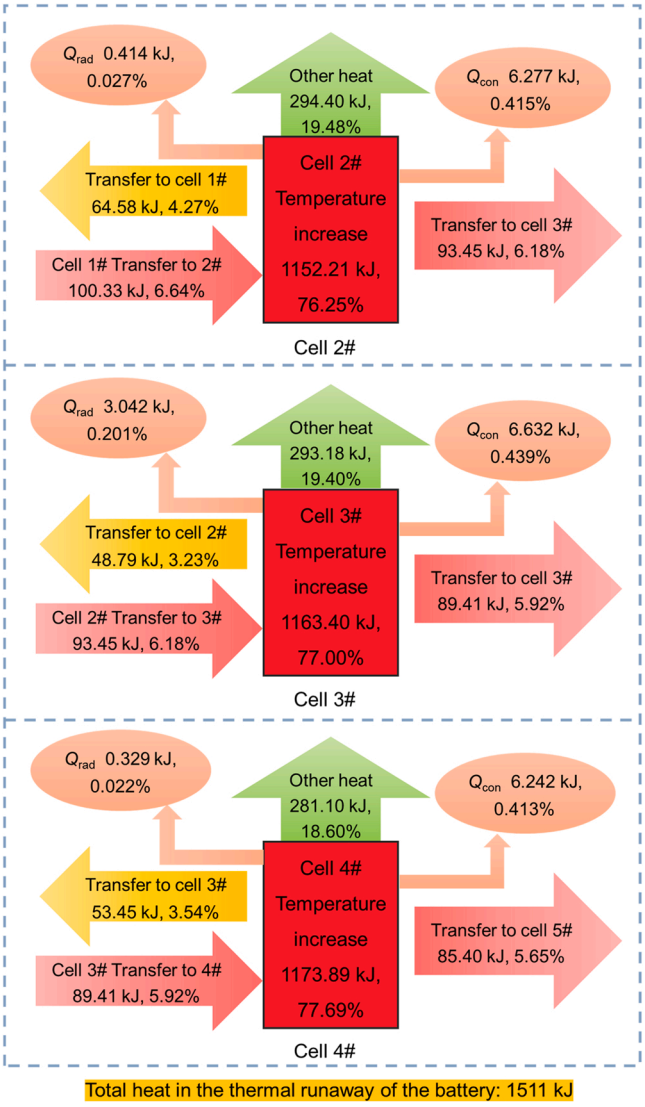

Fig. 11. Energy flow proportions of cell 2#, 3#, and 4# during TRP.

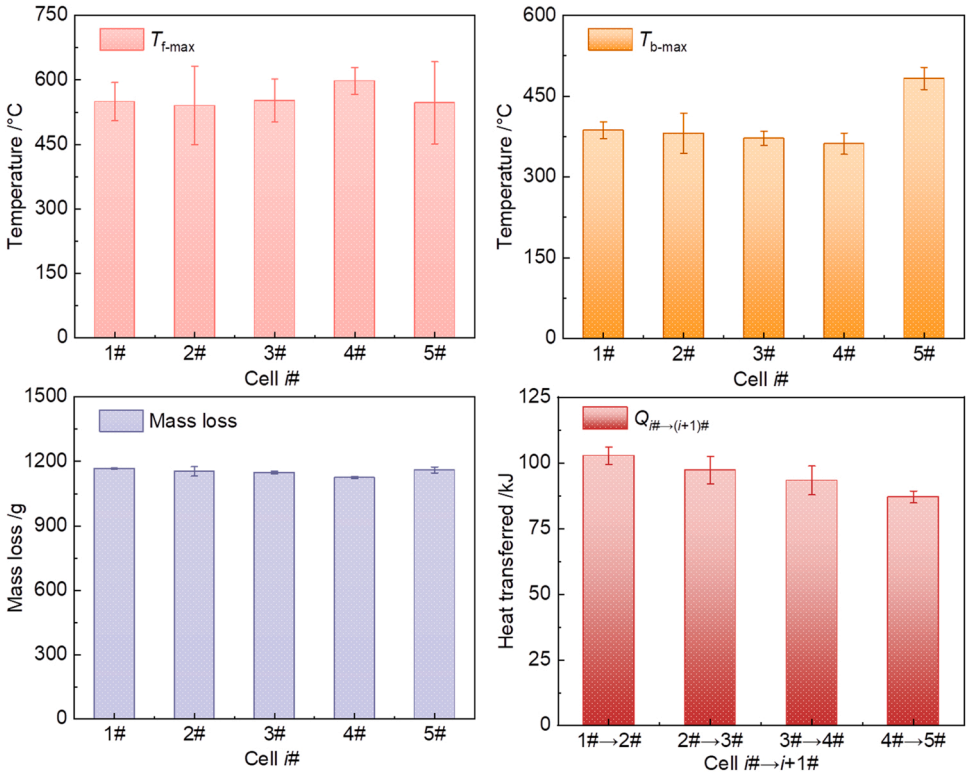

Fig. 12. The error bars of the key parameters.

heat exchange is between 10^{-1} and 1, the energy transferred through heat conduction is in the range of 10^1 to 10^2, and the energy used to heat the cell itself is on the order of 10^3.

To more clearly understand the energy flow of $LiFePO_4$ in the TR process, the energy flow diagram is shown in Fig. 11. In our previous study, the total heat in the thermal runaway of a 280 Ah $LiFePO_4$ battery is calculated to be 1511 kJ. Based on the above calculation results, the energy composition of each cell during TR propagation is normalized to compare the proportion of energy flow distribution. It can be found that more than 75 % of the energy is used to heat the cell itself. The percentage of heat transferred to the next battery is in the range of 5–7 %, while approximately 3.5 % of heat is returned to the previous battery. Only about 0.5 % of the heat is radiated and convected through the upper surface of the cell. Moreover, it can be observed that about 20 % of the energy is carried out by ejecta. The energy composition is similar to Ref. (Lai et al., 2021). This can be illustrated by the fact that the TR can be triggered when less than 10 % of the energy is transferred to an adjacent cell for the large-format lithium iron phosphate battery. To delay or avoid TRP during the operation of the energy storage station, an insulation layer can be added between the cells to ensure safe operation, and the exhaust structure can be improved to prevent the accumulation of gases inside the battery module.

3.2.4. Error analysis

To illustrate the reliability of the experimental results, error analysis was performed on thermal runaway propagation experiments with five cells. To ensure the consistency of experimental conditions, the same batch of fully charged batteries was used for both sets of experiments. The average value and standard deviation of the key parameters are shown in Fig. 12. It can be seen that the standard deviations of some key parameters such as the maximum temperature of the back surface T_{b_max} during thermal runaway of the battery, mass loss, and heat transfer from the large surface $Q_{i\#\rightarrow(i+1)\#}$ are less than 10 %, and the experimental results have high reliability and accuracy. In addition, the standard deviation for the maximum temperature of the cell front surface T_{f_max} is large. This is due to the greater influence of the front surface's high temperature, when the former battery thermal runaway occurs, it will lead to the front surface of the latter battery having a higher temperature. At the same time, the effect of thermal runaway of the battery itself makes the surface maximum temperature deviate more, but every cell's front surface average maximum temperature is in the range of 540 ~ 600 °C and the standard deviation is still less than 20 %.

4. Conclusion

In this study, the TRP behavior for 280 Ah $LiFePO_4$ batteries with different SOCs were comprehensively analyzed in detail. Four TRP experiments were conducted to explore the effect of the SOC on TRP behavior. First, the effect of SOC on TRP is studied. Then, the TRP behavior and characteristics are analyzed through the TRP experiment with five cells. Finally, the energy flow distribution is investigated for large-format LFP. The main conclusions are summarized as follows:

1) For the battery with different SOCs, the TRP phenomenon does not occur for the cell with 40 % and 80 % SOC. All TR occurs for three cells with 100 % SOC after the first cell is triggered TR. With the increase of SOC, the safety vent opening time gradually becomes shorter, and the maximum temperature of the cell surface gradually increases when TR occurs. In addition, the average heat transfer power is 118.41 W, 195.91 W, and 264.07 W respectively under different SOCs.
2) In the module consisting of large-format $LiFePO_4$ batteries, the front surface temperature may exceed 500 ℃ after the TRP behavior occurs, while the back surface temperature is approximately 360 ℃ (except for cell 5#). The TRP time interval fluctuates due to the effect of expansion on the contact thermal resistance. The TRP speed is in the range of 0.05–0.12 mm/s. Furthermore, the heat transfer from cell *i*# to (*i* + 1) # is an order of magnitude greater than the heat transfer to (*i*-1) # in terms of the value of the temperature change.

3) According to the energy flow distribution in the TRP process, more than 75 % of the energy is used to heat the cell itself, approximately 20 % is carried out by ejecta, and only about 5~7 % is transferred to the next battery. TR can be triggered when less than 10 % of the energy is transferred to an adjacent cell for large-format LFP.

This work reveals the TRP characteristics of large-format $LiFePO_4$ batteries and clarifies the energy flow distribution of the TRP process. This study can provide some important data and theoretical support for the TR barrier design of large-format $LiFePO_4$ battery modules. At the same time, it can also guide the safety design of electrochemical energy storage stations.

CRediT authorship contribution statement

Laifeng Song: Conceptualization, Data curation, Methodology, Writing – original draft. **Zonghou Huang**: Visualization, Methodology, Validation. **Wenxin Mei**: Writing – review & editing. **Zhuangzhuang Jia:** Investigation, Experimental design. **Yin Yu:** Experiment. **Qingsong Wang:** Writing – review & editing, Supervision, Funding acquisition, and Project administration. **Kaiqiang Jin**: Supervision, Writing – review & editing.

Declaration of Competing Interest

The authors declare that they have no known competing financial interests or personal relationships that could have appeared to influence the work reported in this paper.

Acknowledgements

This work is supported by the National Key R&D Program of China (No. 2021YFB2402001), the China National Postdoctoral Program for Innovative Talents (No. BX20220286), and the China Postdoctoral Science Foundation (No. 2022T150615). Prof. Q.S Wang is supported by Youth Innovation Promotion Association CAS (No. Y201768).

References

Bugryniec, P.J., Davidson, J.N., Cumming, D.J., Brown, S.F., 2019. Pursuing safer batteries: thermal abuse of LiFePO4 cells. J. Power Sources 414, 557–568.
Chen, M., Ouyang, D., Weng, J., Liu, J., Wang, J., 2019. Environmental pressure effects on thermal runaway and fire behaviors of lithium-ion battery with different cathodes and state of charge. Process Saf. Environ. Prot. 130, 250–256.
Duh, Y.-S., Theng, J.-H., Chen, C.-C., Kao, C.-S., 2020. Comparative study on thermal runaway of commercial 14500, 18650 and 26650 LiFePO4 batteries used in electric vehicles. J. Energy Storage 31, 101580.
Feng, X., He, X., Ouyang, M., Lu, L., Wu, P., Kulp, C., Prasser, S., 2015a. Thermal runaway propagation model for designing a safer battery pack with 25 Ah LiNi Co Mn O2 large format lithium ion battery. Appl. Energy 154, 74–91.
Feng, X., Sun, J., Ouyang, M., Wang, F., He, X., Lu, L., Peng, H., 2015b. Characterization of penetration induced thermal runaway propagation process within a large format lithium ion battery module. J. Power Sources 275, 261–273.
Feng, X., Ouyang, M., Liu, X., Lu, L., Xia, Y., He, X., 2018. Thermal runaway mechanism of lithium ion battery for electric vehicles: a review. Energy Stroage Mater. 10, 246–267.
Feng, X., Ren, D., He, X., Ouyang, M., 2020. Mitigating thermal runaway of lithium-ion batteries. Joule 4, 743–770.
Huang, Z., Zhao, C., Li, H., Peng, W., Zhang, Z., Wang, Q., 2020. Experimental study on thermal runaway and its propagation in the large format lithium ion battery module with two electrical connection modes. Energy 205, 117906.
Huang, Z., Li, X., Wang, Q., Duan, Q., Li, Y., Li, L., Wang, Q., 2021a. Experimental investigation on thermal runaway propagation of large format lithium ion battery modules with two cathodes. Int. J. Heat Mass Transf. 172, 121077.
Huang, Z., Liu, J., Zhai, H., Wang, Q., 2021b. Experimental investigation on the characteristics of thermal runaway and its propagation of large-format lithium ion batteries under overcharging and overheating conditions. Energy 233, 121103.
Huang, Z., Yu, Y., Duan, Q., Qin, P., Sun, J., Wang, Q., 2022. Heating position effect on internal thermal runaway propagation in large-format lithium iron phosphate battery. Appl. Energy 325, 119778.
Jia, Y., Uddin, M., Li, Y., Xu, J., 2020. Thermal runaway propagation behavior within 18,650 lithium-ion battery packs: a modeling study. J. Energy Storage 31, 101668.
Jia, Z., Huang, Z., Zhai, H., Qin, P., Zhang, Y., Li, Y., Wang, Q., 2022a. Experimental investigation on thermal runaway propagation of 18,650 lithium-ion battery modules with two cathode materials at low pressure. Energy 251, 123925.
Jia, Z., Qin, P., Li, Z., Wei, Z., Jin, K., Jiang, L., Wang, Q., 2022b. Analysis of gas release during the process of thermal runaway of lithium-ion batteries with three different cathode materials. J. Energy Storage 50, 104302–104311.
Jin, Y., Zheng, Z., Wei, D., Jiang, X., Lu, H., Sun, L., Tao, F., Guo, D., Liu, Y., Gao, J., Cui, Y., 2020. Detection of micro-scale Li dendrite via H2 gas capture for early safety warning. Joule 4, 1714–1729.
Lai, X., Wang, S., Wang, H., Zheng, Y., Feng, X., 2021. Investigation of thermal runaway propagation characteristics of lithium-ion battery modules under different trigger modes. Int. J. Heat Mass Transf. 171, 121080.
Lamb, J., Orendorff, C.J., Steele, L.A.M., Spangler, S.W., 2015. Failure propagation in multi-cell lithium ion batteries. J. Power Sources 283, 517–523.
Lei, B., Zhao, W., Ziebert, C., Uhlmann, N., Rohde, M., Seifert, H., 2017. Experimental analysis of thermal runaway in 18650 cylindrical Li-Ion cells using an accelerating rate calorimeter. Batteries 3, 14.
Li, H., Duan, Q., Zhao, C., Huang, Z., Wang, Q., 2019. Experimental investigation on the thermal runaway and its propagation in the large format battery module with Li (Ni1/3Co1/3Mn1/3)O2 as cathode. J. Hazard Mater. 375, 241–254.
Li, W., Ostanek, J., 2023. Heat transfer experiments and correlations for vent gases emerging from a Li-ion battery and impinging on a flat surface. Int. J. Heat Mass Transf. 200, 123516.
Liu, P., Liu, C., Yang, K., Zhang, M., Gao, F., Mao, B., Li, H., Duan, Q., Wang, Q., 2020. Thermal runaway and fire behaviors of lithium iron phosphate battery induced by over heating. J. Energy Storage 31, 101714.
Liu, P., Li, Y., Mao, B., Chen, M., Huang, Z., Wang, Q., 2021a. Experimental study on thermal runaway and fire behaviors of large format lithium iron phosphate battery. Appl. Therm. Eng. 192, 116949.
Liu, Y., Niu, H., Li, Z., Liu, J., Xu, C., Huang, X., 2021b. Thermal runaway characteristics and failure criticality of massive ternary Li-ion battery piles in low-pressure storage and transport. Process Saf. Environ. Prot. 155, 486–497.
Lopez, C.F., Jeevarajan, J.A., Mukherjee, P.P., 2015. Experimental analysis of thermal runaway and propagation in lithium-ion battery modules. J. Electrochem. Soc. 162, A1905–A1915.
Mao, B., Liu, C., Yang, K., Li, S., Liu, P., Zhang, M., Meng, X., Gao, F., Duan, Q., Wang, Q., Sun, J., 2021. Thermal runaway and fire behaviors of a 300 Ah lithium ion battery with LiFePO4 as cathode. Renew. Sustain. Energy Rev. 139, 110717.
Mathieu, O., Grégoire, C.M., Turner, M.A., Mohr, D.J., Alturaifi, S.A., Thomas, J.C., Petersen, E.L., 2022. Experimental investigation of the combustion properties of an average thermal runaway gas mixture from Li-Ion batteries. Energy Fuels 36, 3247–3258.
Ouyang, D., Liu, J., Chen, M., Wang, J., 2017. Investigation into the fire hazards of lithium-ion batteries under overcharging. Appl. Sci. 7, 1314–1333.
Ping, P., Wang, Q., Huang, P., Li, K., Sun, J., Kong, D., Chen, C., 2015. Study of the fire behavior of high-energy lithium-ion batteries with full-scale burning test. J. Power Sources 285, 80–89.
Qin, P., Jia, Z., Wu, J., Jin, K., Duan, Q., Jiang, L., Sun, J., Ding, J., Shi, C., Wang, Q., 2022. The thermal runaway analysis on LiFePO4 electrical energy storage packs with different venting areas and void volumes. Appl. Energy 313, 118767–118777.
Sun, H., Zhang, L., Duan, Q., Wang, S., Sun, S., Sun, J., Wang, Q., 2022. Experimental study on suppressing thermal runaway propagation of lithium-ion batteries in confined space by various fire extinguishing agents. Process Saf. Environ. Prot. 167, 299–307.
Wang, Cj, Zhu, Yl, Gao, F., Qi, C., Zhao, Pl, Meng, Qf, Wang, Jy, Wu, Qb, 2020. Thermal runaway behavior and features of LiFePO4 graphite aged batteries under overcharge. Int. J. Energy Res. 44, 5477–5487.
Wang, F., Harindintwali, J.D., Yuan, Z., Wang, M., Wang, F., Li, S., Yin, Z., Huang, L., Fu, Y., Li, L., Chang, S.X., Zhang, L., Rinklebe, J., Yuan, Z., Zhu, Q., Xiang, L., Tsang, D.C.W., Xu, L., Jiang, X., Liu, J., Wei, N., Kastner, M., Zou, Y., Ok, Y.S., Shen, J., Peng, D., Zhang, W., Barcelo, D., Zhou, Y., Bai, Z., Li, B., Zhang, B., Wei, K., Cao, H., Tan, Z., Zhao, L.B., He, X., Zheng, J., Bolan, N., Liu, X., Huang, C., Dietmann, S., Luo, M., Sun, N., Gong, J., Gong, Y., Brahushi, F., Zhang, T., Xiao, C., Li, X., Chen, W., Jiao, N., Lehmann, J., Zhu, Y.G., Jin, H., Schaffer, A., Tiedje, J.M., Chen, J.M., 2021a. Technologies and perspectives for achieving carbon neutrality. Innovation 2, 100180.
Wang, H., Xu, H., Zhao, Z., Wang, Q., Jin, C., Li, Y., Sheng, J., Li, K., Du, Z., Xu, C., Feng, X., 2022a. An experimental analysis on thermal runaway and its propagation in Cell-to-Pack lithium-ion batteries. Appl. Therm. Eng. 211, 118418.
Wang, Q., Huang, P., Ping, P., Du, Y., Li, K., Sun, J., 2017. Combustion behavior of lithium iron phosphate battery induced by external heat radiation. J. Loss Prev. Process Ind. 49, 961–969.
Wang, Q., Mao, B., Stoliarov, S.I., Sun, J., 2019. A review of lithium ion battery failure mechanisms and fire prevention strategies. Prog. Energy Combust. Sci. 73, 95–131.
Wang, W., He, T., He, S., You, T., Khan, F., 2021b. Modeling of thermal runaway propagation of NMC battery packs after fast charging operation. Process Saf. Environ. Prot. 154, 104–117.
Wang, Z., Chen, S., He, X., Wang, C., Zhao, D., 2022b. A multi-factor evaluation method for the thermal runaway risk of lithium-ion batteries. J. Energy Storage 45, 103767.
Yan, W., Wang, Z., Chen, S., 2021. Quantitative analysis on the heat transfer modes in the process of thermal runaway propagation in lithium-ion battery pack under confined and semi-confined space. Int. J. Heat Mass Transf. 176, 121483.
Yuan, L., Dubaniewicz, T., Zlochower, I., Thomas, R., Rayyan, N., 2020. Experimental study on thermal runaway and vented gases of lithium-ion cells. Process Saf. Environ. Prot. 144, 186–192.

Zhai, H., Li, H., Ping, P., Huang, Z., Wang, Q., 2021. An experimental-based Domino prediction model of thermal runaway propagation in 18,650 lithium-ion battery modules. Int. J. Heat. Mass Transf. 181, 122024.
Zhang, Y., Mei, W., Qin, P., Duan, Q., Wang, Q., 2021. Numerical modeling on thermal runaway triggered by local overheating for lithium iron phosphate battery. Appl. Therm. Eng. 192, 116928–116936.
Zhao, C., Wang, T., Huang, Z., Wu, J., Zhou, H., Ma, M., Xu, J., Wang, Z., Li, H., Sun, J., Wang, Q., 2021. Experimental study on thermal runaway of fully charged and overcharged lithium-ion batteries under adiabatic and side-heating test. J. Energy Storage 38, 102519.
Zhou, Z., Zhou, X., Wang, D., Li, M., Wang, B., Yang, L., Cao, B., 2021. Experimental analysis of lengthwise/transversal thermal characteristics and jet flow of large-format prismatic lithium-ion battery. Appl. Therm. Eng. 195, 117244.
Zhou, Z., Zhou, X., Wang, B., Liew, K.M., Yang, L., 2022. Experimentally exploring thermal runaway propagation and prevention in the prismatic lithium-ion battery with different connections. Process Saf. Environ. Prot. 164, 517–527.